Original Article

MOLECULAR METABOLISM

Loss of *Tbk1* kinase activity protects mice from diet-induced metabolic dysfunction

Victoria H. Cruz [1], Emily N. Arner [1], Katherine W. Wynne [1], Philipp E. Scherer [2], Rolf A. Brekken [1,3,*]

ABSTRACT

Objective: TANK Binding Kinase 1 (TBK1) has been implicated in the regulation of metabolism through studies with the drug amlexanox, an inhibitor of the IκB kinase (IKK)-related kinases. Amlexanox induced weight loss, reduced fatty liver and insulin resistance in high fat diet (HFD) fed mice and has now progressed into clinical testing for the treatment and prevention of obesity and type 2 diabetes. However, since amlexanox is a dual IKKε/TBK1 inhibitor, the specific metabolic contribution of TBK1 is not clear.

Methods: To distinguish metabolic functions unique to TBK1, we examined the metabolic profile of global *Tbk1* mutant mice challenged with an obesogenic diet and investigated potential mechanisms for the improved metabolic phenotype.

Results and conclusion: We report that systemic loss of TBK1 kinase function has an overall protective effect on metabolic readouts in mice on an obesogenic diet, which is mediated by loss of an inhibitory interaction between TBK1 and the insulin receptor.

Keywords TBK1; IKKε; Obesity; Insulin; Insulin resistance; Metabolism

1. INTRODUCTION

The prevalence of obesity has expanded dramatically over the last 30 years worldwide and has contributed to the increasing health burden of associated complications, including insulin resistance, type 2 diabetes, cardiovascular disease, hypertension, liver steatosis and dyslipidemia [1–3]. A primary pathology of obesity and metabolic disorders is the induction of chronic low-grade, unresolved inflammation in organs pertinent to energy homeostasis. This so-called "meta-inflammation" consists of increased levels of proinflammatory cytokines and macrophage infiltration in white adipose tissue (WAT) and is coincident with the manifestation of insulin resistance [4–6]. While the etiology of insulin resistance is complicated and multifaceted, numerous studies have demonstrated that blocking inflammatory mediators through genetic or pharmacological means results in improved insulin and glucose tolerance [7–12].

NF-κB is a major transcriptional driver of inflammation that is activated in response to cytokines and pathogenic stimuli to promote the upregulation of inflammatory and immune regulatory gene expression. Not surprisingly, NF-κB is chronically active in many inflammatory diseases and over the past two decades has gained significant attention in the metabolism field due to its high-level activity in affected tissues [13,14]. Most metabolic studies have centered on canonical NF-κB activators, such as IKKα and IKKβ; however, Chiang and colleagues [14] reported that the noncanonical activators, IKKε and TBK1, are more highly expressed than canonical activators in metabolically affected tissues of obese animals. Subsequent investigations revealed that *Ikbke*$^{-/-}$ mice and mice treated with amlexanox (a dual IKKε/TBK1 small molecule inhibitor) are protected from diet-induced obesity (DIO) and associated metabolic syndrome conditions [14,15]. This protection is thought to result from loss of TBK1 and IKKε metabolic functions in repressing adaptive energy expenditure in a diet-driven inflammatory state. Due to the embryonic lethality of *Tbk1*$^{-/-}$ mice and the nature of amlexanox as a dual IKKε and TBK1 inhibitor, distinguishing metabolic functions unique to TBK1 remains a challenge [16]. As amlexanox enters the clinical space for the treatment of obesity and type 2 diabetes in human trials, it has become increasingly important to understand the implications of systemic TBK1 inhibition during metabolic stress.

We set out to investigate TBK1-dependent contributions to metabolism in a metabolically challenged rodent model. We did this utilizing a *Tbk1* mutant mouse that harbors two copies of a null *Tbk1* allele (*Tbk1*$^{\Delta/\Delta}$) [17]. This particular "null allele" encodes a truncated TBK1 protein that is catalytically inactive and expressed at low levels, thereby allowing analysis of global TBK1 kinase loss in vivo. Recently, Zhao and colleagues [18] reported the metabolic effects of an adipocyte specific *Tbk1*-deficient animal model. Here, we focus on the analysis of a global loss-of-function mutant, which provides an opportunity to evaluate the function of TBK1 in a wider context than just the adipocyte.

We report that *Tbk1*$^{\Delta/\Delta}$ mice are resistant to high fat diet-induced weight gain and pancreatic islet hyperplasia and hypertrophy. Additionally, we found that TBK1 inhibits insulin receptor signaling in the HFD setting, a function that is absent in *Tbk1*$^{\Delta/\Delta}$ animals. As a result,

[1]Division of Surgical Oncology, Department of Surgery and the Hamon Center for Therapeutic Oncology Research, USA [2]Touchstone Diabetes Center, Department of Internal Medicine, USA [3]Department of Pharmacology, University of Texas Southwestern Medical Center, Dallas, TX, 75390, USA

*Corresponding author. Hamon Center for Therapeutic Oncology Research, University of Texas Southwestern Medical Center, 6000 Harry Hines Blvd., Dallas, TX, 75390-8593, USA. Fax: +214 648 4940. E-mail: rolf.brekken@utsouthwestern.edu (R.A. Brekken).

Received April 23, 2018 • Revision received May 30, 2018 • Accepted June 7, 2018 • Available online 11 June 2018

https://doi.org/10.1016/j.molmet.2018.06.007

Abbreviations

AKT	Protein kinase B
ATKO	Adipose tissue knockout
DIO	Diet-induced obesity
GAPDH	Glyceraldehyde 3-phosphate dehydrogenase
GSK3β	Glycogen synthase kinase 3β
HFD	High fat diet
IgG	Immunoglobulin G
IKK	IκB kinase
IKKα	IκB kinase α
IKKβ	IκB kinase β
IKKε	IκB kinase ε
IL-12	Interleukin 12
IL-1R	Interleukin 1 receptor
IL-1β	Interleukin 1β
IL-6	Interleukin 6
IRF3	Interferon regulator factor 3
IRS	Insulin receptor substrate
IRβ	Insulin receptor β
IκB	Inhibitor of nuclear factor kappa B
JNK	Jun N-terminal kinase
LPS	Lipopolysaccharide
ND	Normal chow diet
NF-κB	Nuclear factor kappa B
OGTT	Oral glucose tolerance test
p65	NF-κB p65 subunit
PGC-1α	PPARG co-activator 1 alpha
PKC	Protein kinase C
PPARG	Peroxisome proliferator-activated receptor gamma
qPCR	Quantitative polymerase chain reaction
S6K	p70 S6 kinase
SEM	Standard error of the mean
STING	Stimulator of interferon genes
TANK	TRAF family member associated NF-κβ activator
TBK1	TANK binding kinase 1
TNFα	Tumor necrosis factor-alpha
UCP1	Uncoupling protein 1
UCP2	Uncoupling protein 2
WAT	White adipose tissue
WT	Wild-type

HFD-fed *Tbk1*$^{\Delta/\Delta}$ mice are more responsive to insulin compared to *Tbk1*$^{+/+}$ mice, as seen by their more efficient glucose absorption, greater AKT activity and higher levels of insulin receptor substrate (IRS) protein. Accordingly, *Tbk1*$^{\Delta/\Delta}$ mice are more active and have greater energy expenditure relative to *Tbk1*$^{+/+}$ mice, accounting for their leaner body composition. Consistent with an improved metabolic phenotype, *Tbk1*$^{\Delta/\Delta}$ mice also display reduced inflammation in liver and WAT compared to *Tbk1*$^{+/+}$ mice post HFD. Taken together, our results describe a healthier phenotype with global loss of TBK1 kinase function under metabolic challenge and highlight the suitability of TBK1 as a therapeutic target in the prevention and treatment of type 2 diabetes and obesity.

2. MATERIALS AND METHODS

2.1. Animals

Tbk1$^{\Delta/\Delta}$ mice were generated in a pure 129S5 strain as previously described [17] and were generously provided by Pfizer (Cambridge, MA). *Tbk1*$^{\Delta/\Delta}$ mice, *Tbk1*$^{+/+}$ littermates and C57BL/6 mice were bred and maintained in a pathogen-free barrier facility with access to food and water *ad libitum*. All protocols for mouse use and euthanasia were reviewed and approved by the Institutional Animal Care and Use Committee of the University of Texas Southwestern Medical Center (Dallas, TX).

2.2. Animal studies

All experiments were conducted using littermate-controlled male mice. HFD experiments were initiated at 4 weeks of age. Mice were fed a normal chow diet (16% protein diet, irradiated) (Teklad Global Diets; Envigo, East Millstone, NJ), or a 60% HFD (D12492; Research Diets, Inc., New Brunswick, NJ). Tissue and blood were collected in the fasted state. Before the metabolic cage studies, the mice were housed individually in metabolic chambers for 1 week for acclimation. Metabolic measurements were obtained continuously using TSE metabolic chambers (TSE Labmaster System; TSE Systems, Bad Homburg, Germany) in an open-circuit indirect calorimetry system where the mice had access to water and either ND or 60% HFD *ad libitum*. The fat mass and the bone-free lean body composition were measured in nonanesthetized mice using an Echo 3-in-1 nuclear magnetic resonance (MRI) mini Spec instrument (Bruker, Rheinstetten, Germany). For oral glucose tolerance tests (OGTTs), mice were fasted for 4 h prior to administration of glucose (2 g/kg body weight by oral gavage). Mice did not have access to food throughout the experiment. Blood from the tail was measured for glucose content using Contour glucometer strips (Bayer) at 0, 15, 30, 60, 90 and 120 min post oral gavage. Blood was collected and prepared for plasma to measure the concentration of leptin at 0 min and insulin at 0, 15, 30, 60, 90 and 120 min post oral gavage with commercial ELISA kits (Millipore, Burlington, MA). For insulin signaling assays, mice were fasted overnight for insulin injection the next day by i.p. (1 U/kg body weight, insulin). At 15 min post insulin injection, mice were sacrificed and tissues (liver, subcutaneous WAT, skeletal muscle) were harvested and immediately snap-frozen in liquid nitrogen.

2.3. RNA isolation and quantitative RT-PCR

Tissues were excised from mice and snap-frozen with liquid nitrogen. Total RNA was isolated after tissue homogenization in TRIzol (Thermo Fisher, Waltham, MA) and RNA extraction was performed using an RNeasy RNA extraction kit (Qiagen, Germantown, MD). RNA was quantified using a NanoDrop instrument (Thermo Fisher). Complementary DNA was prepared by reverse transcribing 1 μg of RNA with iScript cDNA synthesis kit (Bio-Rad, Hercules, CA). Supplementary Table 1 lists the primer sets used for quantitative RT-PCR. qPCR was performed on a CFX96 Touch Real-Time PCR Detection System (Bio-Rad), with iQ SYBR Green Supermix (Bio-Rad). Results were measured using the comparative threshold cycle (*Ct*) method, with β-actin used for normalization. Fold changes and statistical significance were calculated from three independent replicates.

2.4. Immunoblotting

Tissues were lysed in ice-cold RIPA buffer (50 mM Tris-Cl, 150 mM NaCl, 1% Nonidet P-40, 0.5% sodium deoxycholate, and 0.1% SDS)

containing cocktails of protease (Thermo Fisher Scientific) and phosphatase inhibitors (Sigma—Aldrich, St. Louis, MO) and centrifuged for 20 min at 13,000 $\times$ *g* at 4 °C. Total protein concentration was calculated using a bicinchoninic acid assay kit (Thermo Fisher Scientific). Proteins were resolved by SDS-PAGE and transferred to a methanol-activated polyvinylidene difluoride membrane. All primary and secondary antibodies were diluted in 5% donkey serum in TBS with 0.05% tween. Primary antibodies used included the following: anti-AKT2 (Cell Signaling, #3063), anti-pAKT2(S474) (Cell Signaling, #8599), anti-pGSK3β(S9) (Cell Signaling, #9323), anti-GSK3β (Cell Signaling, #9315), anti-IL1β (Abcam, ab34837), anti-IL6 (Epitomics, 1957-1), anti-IRβ (Cell Signaling, #3025), anti-pIRβ(S994) (Thermo Fisher, purified custom antibody), anti-IRF3 (Santa Cruz Biotechnology, sc-9082), anti-pIRF3(S396) (Cell Signaling, #4947), anti-IRS1 (Cell Signaling, #3407), anti-p65 (Santa Cruz, sc-109), anti-pp65(S536) (Cell Signaling, #3031), anti-pTBK1(S172) (Cell Signaling, #5483), anti-TBK1 (Abcam, ab40676). Anti-β-actin (Sigma—Aldrich, A2066) and anti-GAPDH (Cell Signaling, #2118) were used as loading controls for all western blots shown. Horseradish peroxidase-conjugated donkey anti-rabbit IgG (1:10,000; Jackson ImmunoResearch Laboratories, West Grove, PA) was used as a secondary antibody. Membranes were exposed with Clarity Western ECL Blotting Substrate (Bio-Rad) and visualized with the Odyssey Fc imager (LI-COR Biotechnology, Lincoln, NE).

2.5. Immunoprecipitation

Briefly, liver tissue lysates were prepared by lysis in TNET buffer (150 mM NaCl, 5 mM EDTA, 50 mM Tris ph 8.0, 1% Triton X) plus protease and phosphatase inhibitor cocktails (Thermo Scientific) and 1 mM PMSF. Liver tissue lysate concentrations were assayed using a bicinchoninic acid assay and then equilibrated with lysis buffer. Lysates were pre-cleared by incubation with 20 μL of Protein A/G agarose beads (Thermo Scientific) for 90 min at 4 °C followed by centrifugation. Pre-cleared lysates (250 μg/sample) were then incubated with rabbit anti-TBK1 (Cell Signaling, #3031) or rabbit IgG control (Cell Signaling, #2729) and 30 μL of Protein A/G agarose beads and rotated overnight at 4 °C. Immunoprecipitates were washed three times in TNET buffer then heated to 95 °C for 5 min in standard SDS sample buffer. Samples were separated by SDS-PAGE followed by western blot analysis.

2.6. Histology and immunohistochemistry

Fat pads, livers, and pancreas tissues were excised and either frozen in liquid nitrogen and embedded in optimum cutting temperature compound (OCT, Tissue-Tek; EMS, Hatfield, PA) for frozen sections or fixed with 10% neutral buffered formalin solution overnight and embedded in paraffin for sectioning. Frozen liver sections (10 μm) were air-dried overnight and then fixed in 10% neutral buffered formalin for 10 min at room temperature. After brief rinsing with water and then 60% isopropanol, frozen liver sections were stained with oil red O for 15 min and counterstained with hematoxylin. Formalin-fixed paraffin embedded fat pads and pancreas tissues were cut into 5 μm sections. Paraffin sections were deparaffinized and rehydrated with xylene and serial dilutions of ethanol followed by H&E stain or antigen retrieval with 0.01 mol/L citric acid buffer (pH 6.0) for immunohistochemistry. Sections for immunohistochemical analysis were blocked with 20% aquablock and incubated with rabbit anti-cd11b/c (Novus Biologicals, NB110-40766) in blocking solution (5% BSA in TBS with 0.05% tween) at 4 °C overnight. Horseradish peroxidase—conjugated donkey anti-rabbit IgG (Jackson ImmunoResearch Laboratories, West Grove, PA) was used as a secondary antibody. Negative controls included omission of primary antibody. All slides were visualized with a Nikon Eclipse E600 microscope (Nikon, Melville, NY) and color images were captured using a Nikon Digital Dx1200me camera and ACT-1 software. Images were analyzed using NIS Elements AR 2.3 Software (Nikon).

2.7. Statistics

Statistical analyses were performed using GraphPad Prism (GraphPad, La Jolla, CA). Results are expressed as mean ± SEM. All data were analyzed by *t*-test or ANOVA. Significance was accepted at $p < 0.05$, with asterisks denoting *p*-value levels: *, $p < 0.05$; **, $p < 0.01$; ***, $p < 0.001$; and ****, $p < 0.0001$.

3. RESULTS

3.1. HFD induces TBK1 expression and activity

Prolonged consumption of a HFD results in increased expression of IKKε and TBK1 in murine liver and WAT [14,15]. To confirm and extend these results, we evaluated IKKε and TBK1 expression in liver and subcutaneous WAT tissue collected from HFD-fed C57BL/6 mice. Consistent with earlier reports, TBK1 mRNA levels increased nearly 6- and 3-fold, respectively, in liver and WAT of HFD-fed animals (Figure 1A,B). Surprisingly, IKKε transcript levels were not elevated in either set of tissues post HFD, even though IL-6, which is known to be abundant in obese settings, was increased in liver and WAT, confirming the presence of metabolic inflammation in these HFD-fed animals [19,20]. In addition to confirming TBK1 induction at the protein level in liver tissues, we also observed an increase in TBK1 activity as seen by higher levels of pTBK1 and downstream TBK1 targets, pIRF3 and pp65 (Figure 1C). Interestingly, a previous study [21] reported that TBK1 interacts with insulin receptor β subunit (IRβ) in livers of obese rats. Concurrent with elevated TBK1 activity, we also detected a robust increase in IRβ-associated TBK1 by co-immunoprecipitation in liver lysates from HFD-fed mice compared to normal chow diet (ND) animals (Figure 1D). This heightened association could be indicative of a novel insulin-related function for TBK1.

3.2. *Tbk1*$^{\Delta/\Delta}$ mice are resistant to DIO

Upon observing the induction of TBK1 expression, activity and IRβ interaction on HFD feeding, we sought to resolve TBK1 contributions to metabolism that are distinct from its homolog, IKKε. We did this by utilizing *Tbk1*$^{\Delta/\Delta}$ animals [17]. To examine the outcome of metabolic stress in a *Tbk1*-deficient setting, we placed *Tbk1*$^{\Delta/\Delta}$ and *Tbk1*$^{+/+}$ mice on HFD for 10 weeks. Weight measurements for each group were collected weekly and compared to age-matched ND-fed *Tbk1*$^{\Delta/\Delta}$ and *Tbk1*$^{+/+}$ mice (Figure 2A). By 8 weeks of age (4 weeks in the study), we documented a 25% increase in total body weight in HFD-fed *Tbk1*$^{+/+}$ mice compared to ND. Similar to HFD-fed *Ikbke*$^{-/-}$ mice and amlexanox-treated mice, *Tbk1*$^{\Delta/\Delta}$ mice showed only a modest increase in total body weight on HFD relative to ND-fed mice and overall maintained significantly lighter body weights than HFD-fed *Tbk1*$^{+/+}$ mice through the end of the study (Figure 2A,B). To confirm that these differences in body weight and fat mass are not due to *Tbk1*$^{\Delta/\Delta}$ mice eating less than *Tbk1*$^{+/+}$ mice, we evaluated daily food intake relative to body weight. While no significant difference was observed, *Tbk1*$^{\Delta/\Delta}$ mice showed a minor increase in the ratio of HFD intake to body weight, eliminating the possibility of reduced consumption (Figure 2C). Additionally, there were no differences in body weight and length between ND-fed *Tbk1*$^{\Delta/\Delta}$ and *Tbk1*$^{+/+}$ mice, indicating that the resistance to the DIO phenotype seen with *Tbk1*$^{\Delta/\Delta}$ mice is unique to this particular

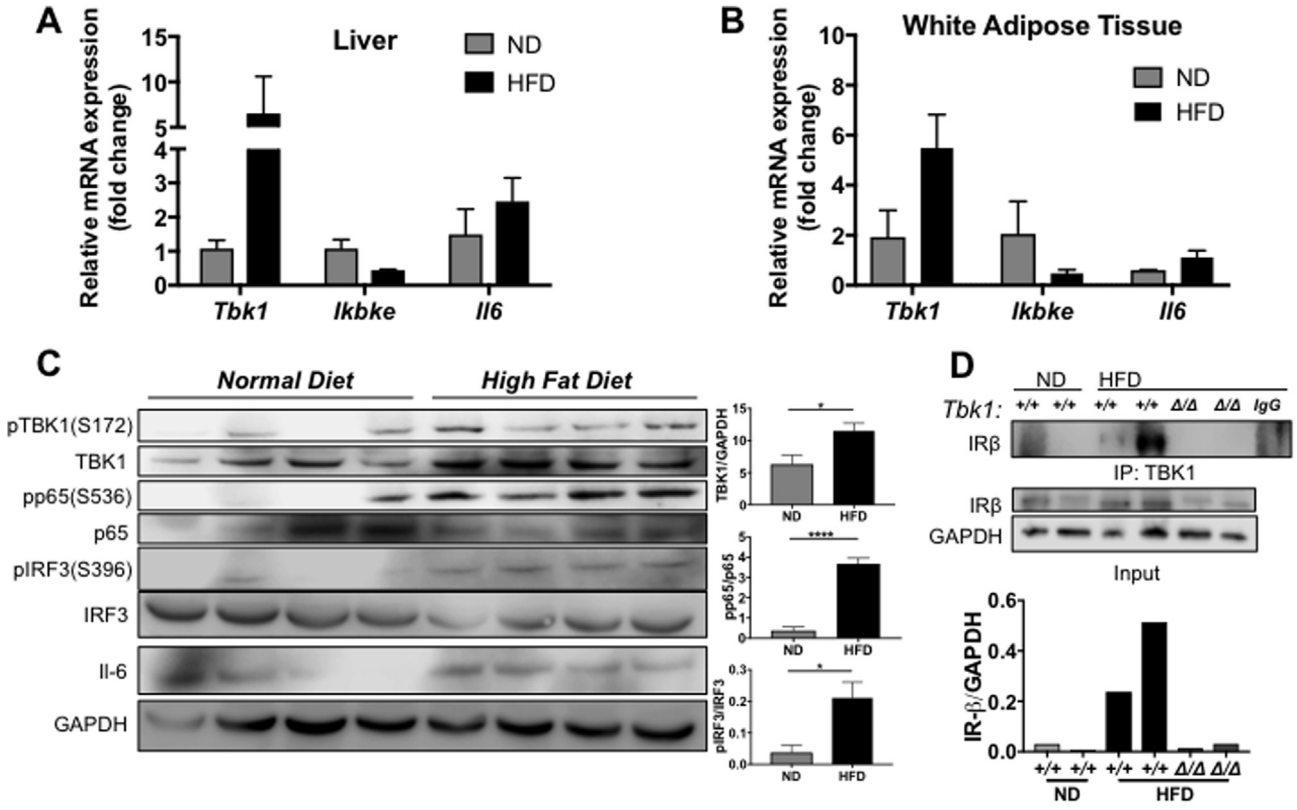

Figure 1: Prolonged consumption of HFD induces TBK1 and promotes interaction with IR. mRNA expression of genes encoding TBK1, IKKε and IL-6 in liver **(A)** and WAT **(B)** of *C57BL/6* mice fed for 10 weeks with HFD or ND as indicated (n = 4 mice/group). Results are representative of mean +/− SEM. Note: p = 0.06 for *Tbk1* expression in WAT between ND and HFD. **(C)** Protein lysates from livers of ND- and HFD-fed *C57BL/6* mice that were fasted overnight were immunoblotted with indicated antibodies and quantified. GAPDH was used as a loading control. **(D)** Liver lysates from ND- or HFD-fed mice were immunoprecipitated with an antibody against TBK1 or IgG, followed by immunoblotting and quantification of IRβ. Normal rabbit IgG was used as a control for specificity (IgG lane). Tissue lysates for immunoprecipitation were immunoblotted with antibodies against IRβ for input and GAPDH as a loading control. Statistical analysis by Student's *t*-test. $*p < 0.05$, $****p < 0.0001$.

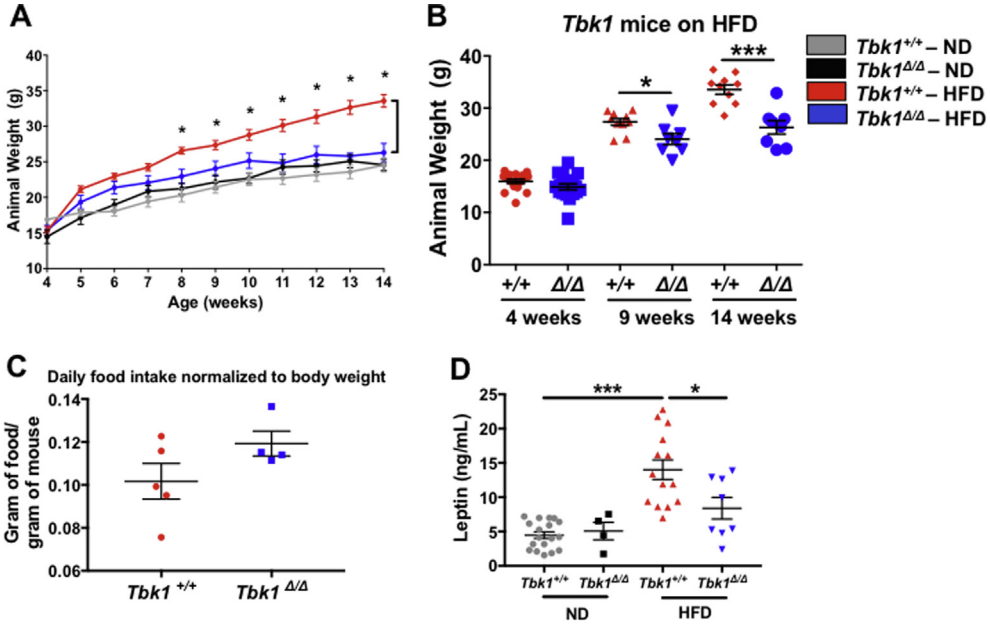

Figure 2: *Tbk1*$^{Δ/Δ}$ mice are protected from HFD-induced weight gain. **(A)** Weekly body weights of *Tbk1*$^{+/+}$ and *Tbk1*$^{Δ/Δ}$ mice fed ND or HFD from 4 to 14 weeks of age (n = 7–10 mice/group). **(B)** Body weights of HFD-fed *Tbk1*$^{+/+}$ and *Tbk1*$^{Δ/Δ}$ mice at 4, 9 and 14 weeks of age. **(C)** Average daily food consumption of 14-week-old HFD-fed *Tbk1*$^{+/+}$ and *Tbk1*$^{Δ/Δ}$ mice was measured as gram of food per gram of mouse. **(D)** Circulating leptin levels were assayed in plasma from *Tbk1*$^{+/+}$ and *Tbk1*$^{Δ/Δ}$ mice as indicated. All mice are from 129S5 background. Results are representative of mean +/− SEM. Statistical analysis by Student's *t*-test. $*p < 0.05$, $***p < 0.001$.

metabolic stress (Supplemental Fig. 1A,B). Next, we analyzed plasma leptin levels, which are usually elevated in obese individuals due to their higher percentage of body fat. We observed approximately a 40% reduction in circulating leptin in HFD *Tbk1*$^{\Delta/\Delta}$ mice relative to *Tbk1*$^{+/+}$ mice, further highlighting the lower percentage of body fat in *Tbk1*$^{\Delta/\Delta}$ mice (Figure 2D).

3.3. *Tbk1*$^{\Delta/\Delta}$ mice are glucose and insulin tolerant on HFD

Given that the association of TBK1 with IRβ was augmented on HFD and that loss of TBK1 protected mice from diet-induced weight gain, we examined the insulin-producing pancreatic beta cells in *Tbk1*$^{+/+}$ and *Tbk1*$^{\Delta/\Delta}$ mice. Increased adipose tissue load resulting from excessive nutrient intake often leads to enhanced demands on pancreatic beta cells for insulin production. Pancreatic islets respond to the greater demand for insulin by increasing in number and in size. HFD-fed *Tbk1*$^{\Delta/\Delta}$ mice were resistant to the increase in islet number and size that was observed in HFD-fed *Tbk1*$^{+/+}$ mice (Figure 3A–C). These results suggested that *Tbk1*$^{\Delta/\Delta}$ mice are more tolerant of glucose and insulin on HFD compared to *Tbk1*$^{+/+}$ mice. OGTTs were performed in fasted (4 h) ND- and HFD-fed *Tbk1*$^{+/+}$ and *Tbk1*$^{\Delta/\Delta}$ mice. As expected, significantly higher blood glucose measurements were observed in HFD-fed *Tbk1*$^{+/+}$ mice compared with ND-fed mice (*Tbk1*$^{+/+}$ and *Tbk1*$^{\Delta/\Delta}$) during the course of the OGTT. However, in contrast to HFD-fed *Tbk1*$^{+/+}$ mice, the high levels of blood insulin and glucose found in HFD-fed *Tbk1*$^{\Delta/\Delta}$ mice returned to basal values by 60 min and 120 min respectively, post oral gavage of glucose. These results indicate that TBK1 deficiency ameliorates diet-induced pancreatic islet stress and improves systemic glucose homeostasis, which is akin to the phenotype of previously reported *Ikbke*$^{-/-}$ mice and amlexanox-treated animals (Figure 3D,E).

3.4. Loss of TBK1 kinase enhances insulin sensitivity on HFD

Munoz et al. [21] also reported that TBK1 can directly phosphorylate serine 994 (S994) of IRβ in livers from obese rats. This particular serine site can be phosphorylated by the serine kinase, protein kinase C (PKC, isoforms β2 and θ) and has been implicated as an inhibitory phosphorylation site that blocks insulin receptor tyrosine kinase activity and subsequent downstream signaling [22,23]. Within metabolically diseased tissues from obese patients, there is a high level of proinflammatory cytokines that can drive activation of stress kinases, including Jun N-terminal kinase (JNK), IKKβ and PKC [24,25]. These kinases are thought to respond to inflammation by constraining the activity of the insulin receptor directly or indirectly through IRSs via inhibitory phosphorylation, ultimately bringing insulin signaling down to baseline [26–28]. Given that TBK1 is a serine/threonine IKK (IκB kinase) family member that is responsive to inflammatory stimuli and is capable of phosphorylating the insulin receptor, we hypothesized that TBK1 negatively regulates insulin signaling through phosphorylation of S994 on IRβ.

We examined the phosphorylation status of IRβ (S994) in liver tissue from ND- and HFD-fed *Tbk1*$^{+/+}$ and *Tbk1*$^{\Delta/\Delta}$ mice with an antibody specific for pIRβ (S994). A specific pIRβ (S994) signal was detectable only in livers from *Tbk1*$^{+/+}$ mice in the HFD-fed group (Figure 4A). Furthermore, co-immunoprecipitation of TBK1 in liver lysates showed TBK1- IRβ association after HFD feeding and also revealed a pIRβ (S994) band exclusively in HFD *Tbk1*$^{+/+}$ livers (Figure 4B). These

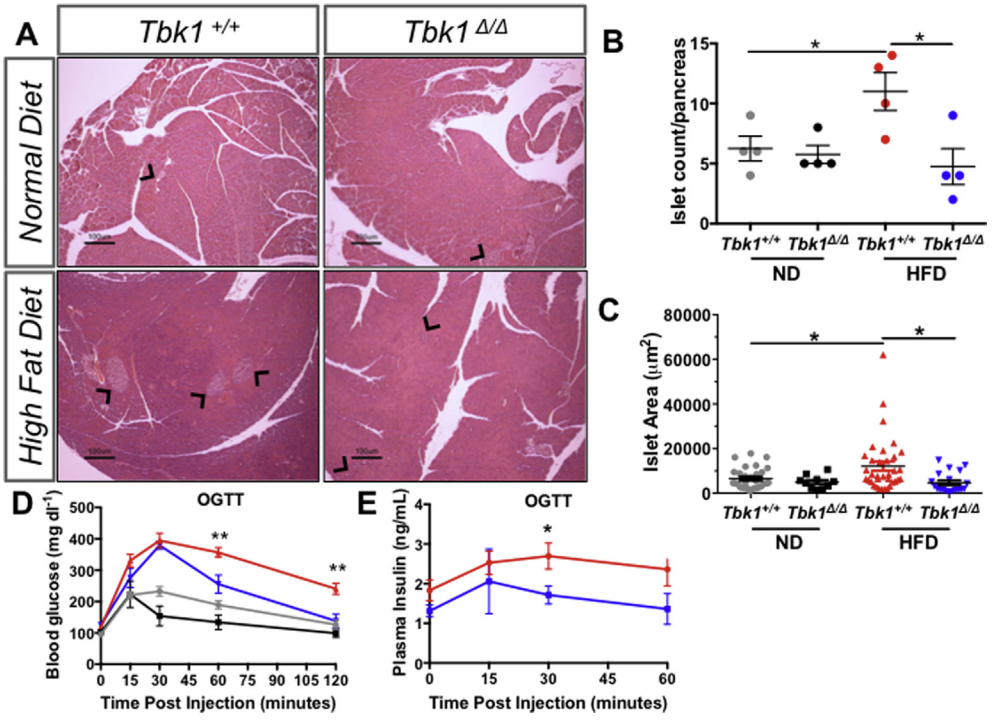

Figure 3: HFD-fed *Tbk1*$^{\Delta/\Delta}$ mice maintain glucose and insulin sensitivity. **(A)** Representative images of pancreata from adult *Tbk1*$^{\Delta/\Delta}$ and *Tbk1*$^{+/+}$ mice after 10 weeks on ND or HFD. Black arrows point to pancreatic islets. Scale bar indicates 100 μM. **(B)** Number of islets counted per pancreas (4x section) in *Tbk1*$^{\Delta/\Delta}$ and *Tbk1*$^{+/+}$ mice on ND or HFD (n = 4 mice/group). **(C)** Area of each islet from **(B)** measured in microns^2. **(D)** Blood glucose and **(E)** plasma insulin measurements at indicated times after oral glucose injection for oral glucose tolerance tests in ND- or HFD-fed *Tbk1*$^{\Delta/\Delta}$ and *Tbk1*$^{+/+}$ mice. For blood glucose, n = 4–10 mice/ND group and 8–12 mice/HFD group. For blood insulin, n ≥ 5 mice/group with exception at 15 min where n = 3 mice/group. All mice are from 129S5 background. Results are representative of mean +/− SEM. Statistical analysis by Student's *t*-test. *$p < 0.05$ and **$p < 0.01$ for HFD-fed *Tbk1*$^{+/+}$ mice compared to HFD-fed *Tbk1*$^{\Delta/\Delta}$ mice. *OGTT*, oral glucose tolerance test.

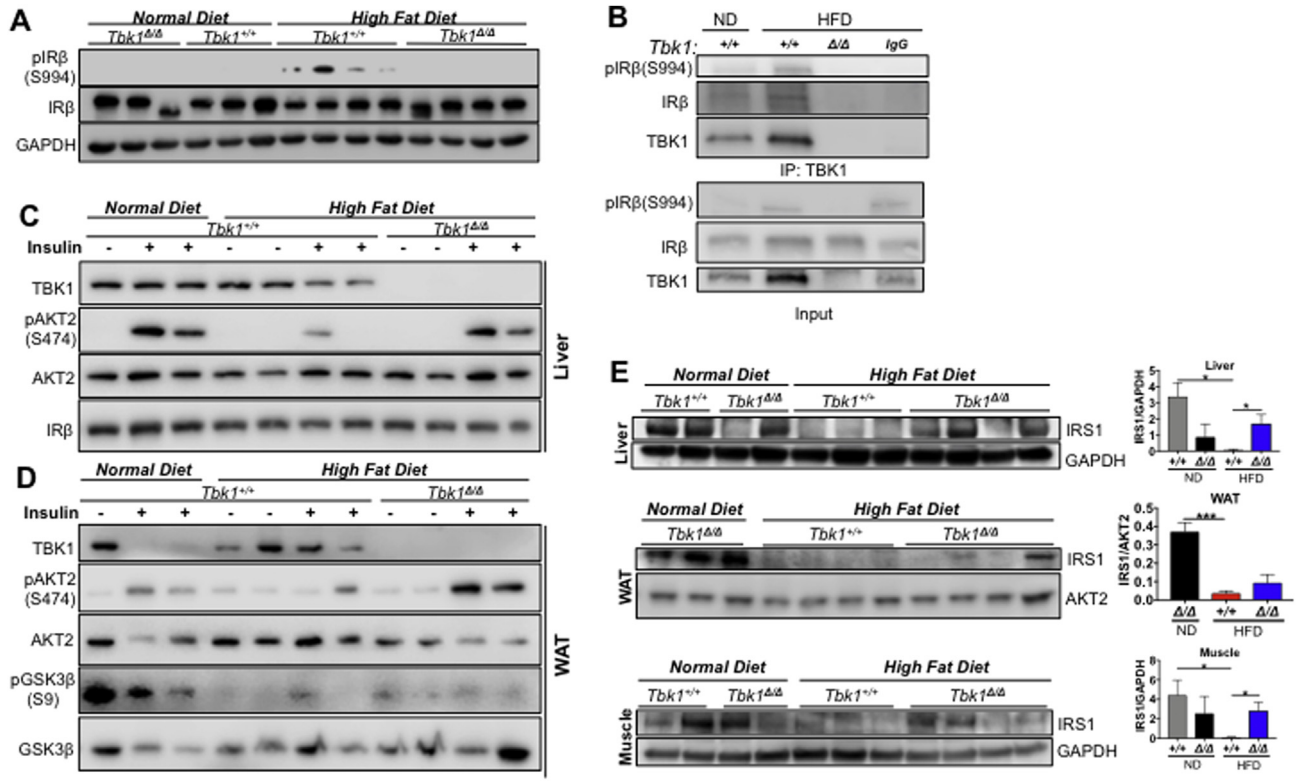

Figure 4: Loss of TBK1 kinase activity diminishes insulin receptor interaction and enhances insulin sensitivity on HFD. **(A)** Liver lysates from ND or HFD-fed *Tbk1*$^{\Delta/\Delta}$ and *Tbk1*$^{+/+}$ mice were probed for pIRβ(S994) and IRβ. GAPDH is shown as a loading control. **(B)** Liver lysates from ND- or HFD-fed *Tbk1*$^{+/+}$ and *Tbk1*$^{\Delta/\Delta}$ mice were immunoprecipitated with an antibody against TBK1 and assayed for IRβ and pIRβ(S994). Normal rabbit IgG was used as a control for specificity (IgG lane). Lysates for immunoprecipitation were immunoblotted with antibodies against pIRβ(S994), IRβ, and TBK1 for input. Liver **(C)** and WAT **(D)** lysates from ND- or HFD-fed *Tbk1*$^{\Delta/\Delta}$ and *Tbk1*$^{+/+}$ mice injected intraperitoneally with insulin (1 U/kg of body weight) or water as a control were probed for indicated proteins. All mice in these experiments were fasted overnight before sacrifice. **(E)** Total IRS1 protein levels in liver, WAT and muscle tissue lysates from 14-week-old HFD-fed *Tbk1*$^{\Delta/\Delta}$ and *Tbk1*$^{+/+}$ mice were detected by immunoblot and quantified. GAPDH, IRβ and AKT2 were used as internal loading controls. All mice are from 129S5 background. Statistical analysis by Student's *t*-test. $^{*}p < 0.05$, $^{***}p < 0.001$.

results confirm that S994 of IRβ is phosphorylated in HFD-fed mouse livers and indicate that TBK1 is likely the upstream kinase responsible. Loss of this inhibitory signal in HFD-fed *Tbk1*$^{\Delta/\Delta}$ tissue suggests that insulin signaling is intact in HFD-fed *Tbk1*$^{\Delta/\Delta}$ animals. We tested this directly by injecting the mice with insulin (1 unit/kg of body weight) or PBS and collected tissues 15 min later for protein isolation. Liver and subcutaneous WAT protein lysates were probed for downstream insulin signaling proteins and phosphoproteins. AKT2 is considered to be the more insulin-responsive isoform of AKT (Protein kinase B, PKB) [29]. In comparison to livers and WAT from ND mice, insulin-induced AKT2 and downstream GSK3β (Glycogen synthase kinase 3β) activation were appreciably lower in HFD *Tbk1*$^{+/+}$ tissues (Figure 4C,D). On the other hand, tissues from insulin-treated HFD *Tbk1*$^{\Delta/\Delta}$ mice maintained consistent AKT2 activation at a level comparable to ND animals. Therefore, loss of TBK1 kinase activity in the context of a metabolic challenge results in the preservation of insulin sensitivity that is normally dampened as a result of HFD.

This difference in insulin sensitivity between *Tbk1*$^{+/+}$ and *Tbk1*$^{\Delta/\Delta}$ mice was confirmed by analysis of total IRS1 protein levels across liver, subcutaneous WAT and skeletal muscle. Persistent inhibitory phosphorylation of IRS1 leads to its degradation and ultimately insulin resistance [27]. In light of the observation that *Tbk1*$^{\Delta/\Delta}$ mice are more responsive to insulin, we suspected they would have more IRS1 protein present in metabolic tissues relative to HFD-fed *Tbk1*$^{+/+}$ mice. In the HFD-fed Tbk1$^{+/+}$ group, there was a consistent loss of detectable IRS1 in all 10 tissues examined. Whereas in HFD fed *Tbk1*$^{\Delta/\Delta}$ mice, IRS1 was easily detectable in 7 out of 12 tissues examined (Figure 4E). Altogether, these findings are consistent with the differences observed in the OGTTs and help to explain why HFD-fed *Tbk1*$^{\Delta/\Delta}$ mice were more glucose tolerant than *Tbk1*$^{+/+}$ mice.

3.5. *Tbk1*$^{\Delta/\Delta}$ mice expend more energy through physical activity

If lack of functional TBK1 on HFD generates greater insulin responsiveness and subsequent glucose absorption in *Tbk1* mutant mice, these animals are likely more efficient in storing and/or expending that energy. Total energy expenditure is composed of voluntary events, such as physical activity, and involuntary events, such as basal metabolic rate and thermogenesis. Thermogenesis was increased in *Ikbke*$^{-/-}$ mice and amlexanox-treated mice compared to control mice and was determined to be the primary difference contributing to their improved phenotype. The expression of thermogenic genes *Ucp1*, *Ucp2*, *Pparg* and *Ppargc1a* were not significantly upregulated in HFD-fed *Tbk1*$^{\Delta/\Delta}$ WAT and livers relative to *Tbk1*$^{+/+}$ mice (Supplemental Fig. 2A,B). However, the thermogenic differences detected in *Ikbke*$^{-/-}$ mice and amlexanox-treated mice were at week 14 of HFD. Considering the 10-week duration of our HFD study, it is possible that differences in thermogenesis were not given sufficient time to manifest.

We evaluated alternative forms of energy expenditure by monitoring *Tbk1*$^{+/+}$ and *Tbk1*$^{\Delta/\Delta}$ mice in metabolic cages over a 72-hour period.

While there were no significant differences between ND-fed groups (Supplemental Fig. 3), HFD-fed *Tbk1*$^{\Delta/\Delta}$ mice were more active than *Tbk1*$^{+/+}$ mice as quantified by their increased movement (beam breaks) throughout the cages (Figure 5A). Accordingly, *Tbk1*$^{\Delta/\Delta}$ mice also had 22% higher oxygen consumption, 25% higher carbon dioxide production and 23% higher heat production, demonstrating greater energy expenditure overall (Figure 5B). Of note, the greatest differences in activity and energy expenditure took place during the dark cycles when the animals were awake. Since mice are nocturnal animals, any differences in resting metabolic rate between the two groups would be apparent during the light or daytime hours. *Tbk1*$^{\Delta/\Delta}$ mice had only a modest increase in movement and energy expenditure during light cycles, indicating that the enhanced nighttime physical activity observed in *Tbk1*$^{\Delta/\Delta}$ mice could account for their increased energy expenditure relative to *Tbk1*$^{+/+}$ mice.

Alongside beam break and energy expenditure measurements, body composition analysis of *Tbk1*$^{+/+}$ and *Tbk1*$^{\Delta/\Delta}$ mice was performed utilizing a nuclear MRI mini spec instrument. Lean and fat mass composition were similar between ND mice, while HFD-fed *Tbk1*$^{+/+}$ animals had 70% more fat mass and 15% less lean mass compared to ND mice (Figure 5C,D). In contrast, HFD-fed *Tbk1*$^{\Delta/\Delta}$ mice contained fat and lean body masses nearly equivalent to ND-fed mice, possibly due in part to their higher energy expenditure. Overall, these findings are in agreement with the insulin and glucose tolerant state of *Tbk1*$^{\Delta/\Delta}$ mice and indicate that they consume more energy via increased activity, accounting for greater lean mass and reduced fat mass.

3.6. HFD-fed *Tbk1*$^{\Delta/\Delta}$ mice maintain lipid homeostasis

Differences in fat mass and lipid accumulation were also examined. HFD induces adipocyte enlargement and proliferation in WAT. In subcutaneous fat pads collected from HFD-fed *Tbk1*$^{+/+}$ mice, we observed larger adipocytes compared to those collected from ND-fed *Tbk1*$^{+/+}$ mice (Figure 6A). While we did see larger adipocytes in fat pads from HFD-fed *Tbk1*$^{\Delta/\Delta}$ mice, overall, they contained a greater abundance of small adipocytes relative to HFD-fed *Tbk1*$^{+/+}$ fat tissue (Figure 6A,B). Additionally, cholesterol levels were measured from plasma of ND- and HFD-fed *Tbk1*$^{+/+}$ and *Tbk1*$^{\Delta/\Delta}$ mice. As expected, a prolonged fat diet led to a nearly 40% increase in circulating cholesterol in *Tbk1*$^{+/+}$ mice (Figure 6C). Yet, *Tbk1*$^{\Delta/\Delta}$ mice maintained cholesterol levels comparable to mice on ND. Furthermore, we performed oil red O staining on frozen liver sections to assess liver steatosis. Consistent with previous results, HFD *Tbk1*$^{+/+}$ mice displayed a striking level of hepatic lipid deposition while *Tbk1*$^{\Delta/\Delta}$ livers showed a 65% reduction in oil red O staining (Figure 6D,E). Despite prolonged consumption of a HFD, *Tbk1*$^{\Delta/\Delta}$

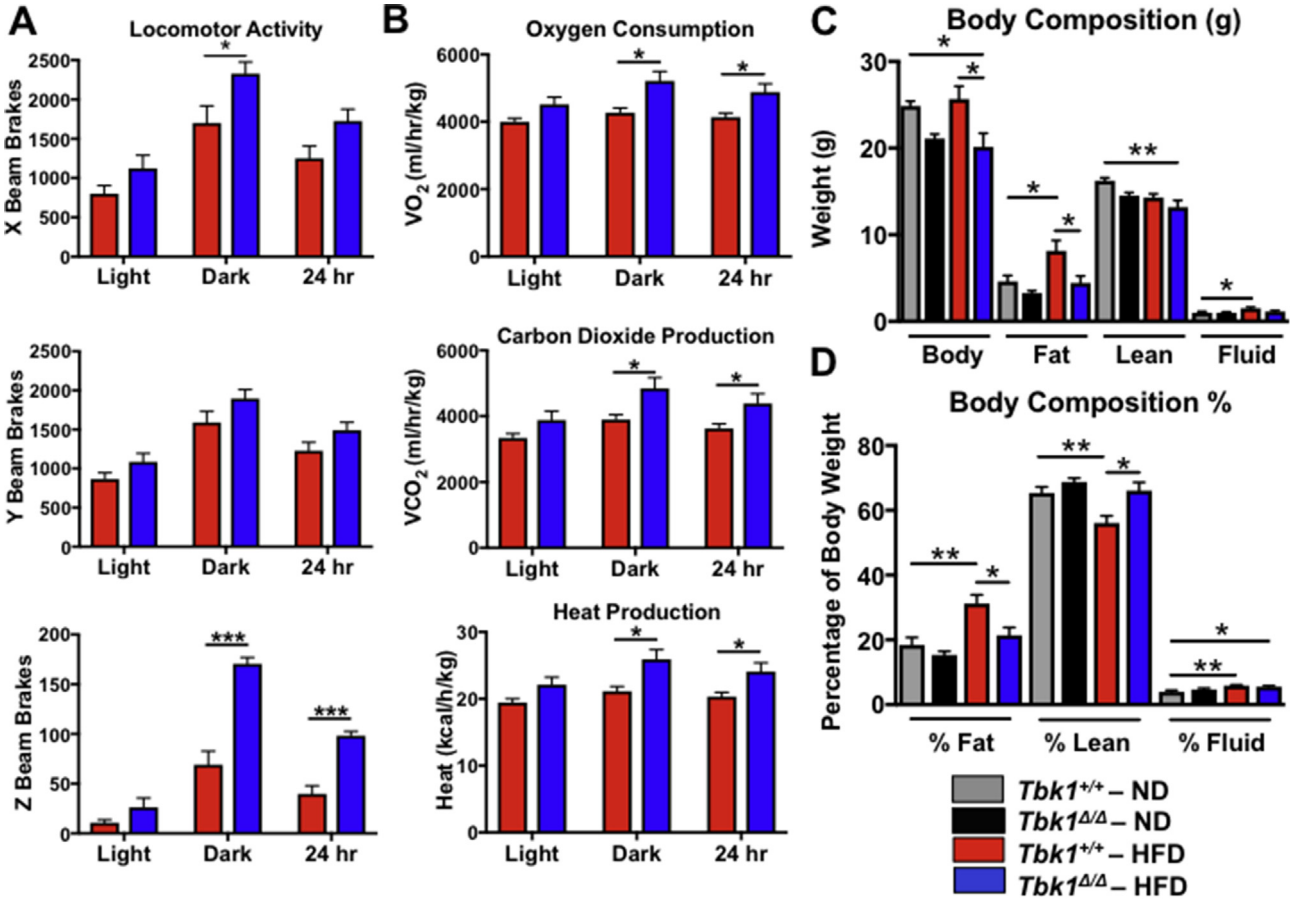

Figure 5: *Tbk1*$^{\Delta/\Delta}$ mice are more active than *Tbk1*$^{+/+}$ mice. Movement throughout the cage **(A)** and energy expenditure measurements **(B)** were collected from 14-week-old *Tbk1*$^{+/+}$ and *Tbk1*$^{\Delta/\Delta}$ mice fed HFD in a metabolic chamber over a 3-day period. **(C)** Total body weight, fat mass, lean mass and fluid in *Tbk1*$^{\Delta/\Delta}$ and *Tbk1*$^{+/+}$ mice fed either ND or HFD at 14 weeks of age. **(D)** Fat and lean mass and bodily fluids as a percentage of total body weight in mice from **(C)**. Results are representative of mean +/− SEM; n = 5 mice/group and all mice are from 129S5 background. Statistical analysis by Student's *t*-test. *$p < 0.05$, **$p < 0.01$, ***$p < 0.001$.

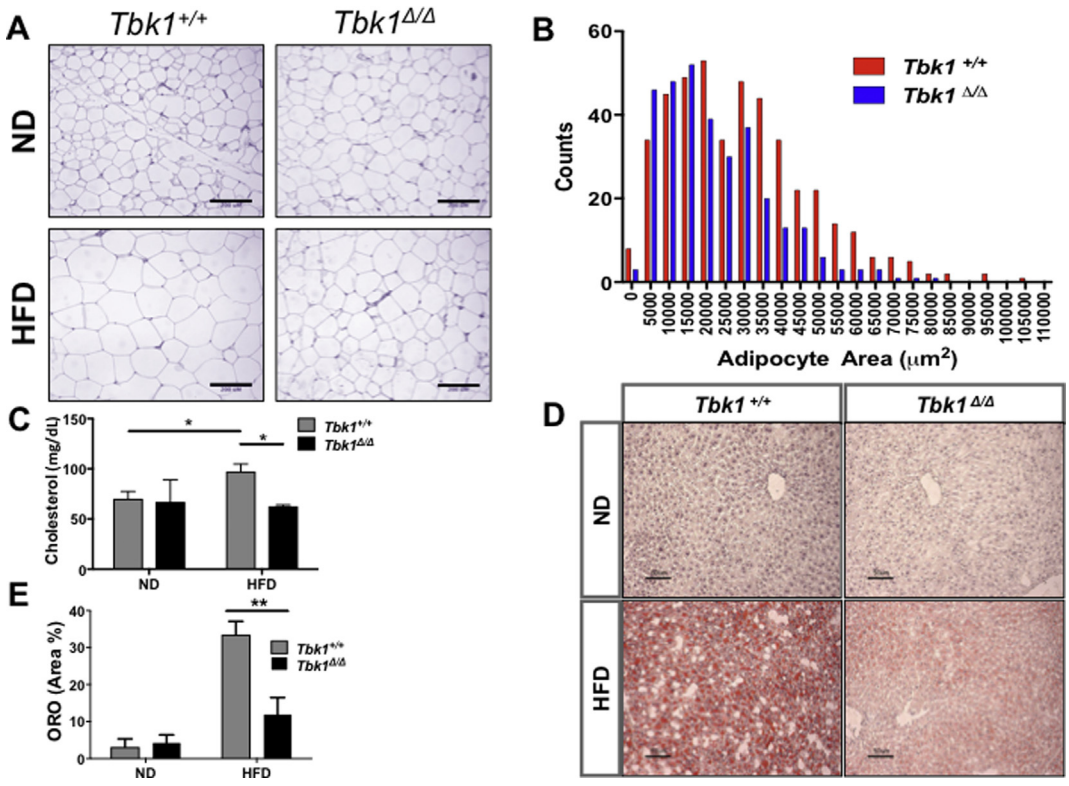

Figure 6: HFD-fed *Tbk1*$^{\Delta/\Delta}$ mice maintain lipid homeostasis. **(A)** Representative 20x images of H&E stained subcutaneous white adipose tissue from *Tbk1*$^{\Delta/\Delta}$ and *Tbk1*$^{+/+}$ mice after 10 weeks on ND or HFD. Scale bar indicates 200 μM. **(B)** Adipocyte area count in fat pads of *Tbk1*$^{\Delta/\Delta}$ and *Tbk1*$^{+/+}$ mice fed HFD (n = 4–8 mice/group). **(C)** Total cholesterol levels were measured in murine plasma using Vitros chemistry systems (Ortho Clinical Diagnostics, Raritan, NJ) (n = 6 mice/group). **(D–E)** Representative images and relative quantification of oil red O stained livers from *Tbk1*$^{\Delta/\Delta}$ and *Tbk1*$^{+/+}$ mice (n = 4–6 mice/group). Scale bar indicates 50 μM. All mice are from 129S5 background. Results are representative of mean +/− SEM. Statistical analysis by Student's *t*-test. *$p < 0.05$, **$p < 0.01$.

mice preserve lipid homeostasis and maintain a consistently healthier phenotype.

3.7. Diet-induced inflammation is nominal in *Tbk1* $^{\Delta/\Delta}$ mice

Chronic low-grade inflammation, also referred to as "meta-inflammation," is a hallmark of metabolic syndrome and strongly associates with insulin resistance. It is characterized by a high degree of immune cell infiltration, primarily macrophages, and local cytokine production in metabolically diseased tissues. Meta-inflammation is thought to stem from pathological adipocyte tissue expansion in an obese state where the tissue becomes poorly oxygenated or hypoxic. Hypoxia leads to fibrosis and necrotic cell death in adipose tissue, which provokes local macrophage activation and/or polarization to an "M1" proinflammatory state. Inflammation is augmented by adipocytes and macrophages that generate proinflammatory cytokines to promote macrophage mobilization from bone marrow and local infiltration into adipose tissue and other metabolically diseased tissues [30].

In light of TBK1's well-established role in mediating innate immunity and *Tbk1*$^{\Delta/\Delta}$ mice being resistant to diet-induced lipogenesis, we suspected *Tbk1*$^{\Delta/\Delta}$ mice would have limited meta-inflammation on HFD. In WAT stained for cd11b/c, we observed quantitatively fewer macrophages in HFD fed *Tbk1*$^{\Delta/\Delta}$ mice relative to *Tbk1*$^{+/+}$ mice (Figure 7A). This difference in macrophage infiltration was confirmed in RNA isolated from WAT of HFD-fed *Tbk1*$^{\Delta/\Delta}$ mice, in which we detected substantial reductions in gene expression of macrophage markers *Cd11c* and *Adgre1* (F4/80) and proinflammatory cytokines *Tnfa*, *Il6* and *Il12* relative to HFD *Tbk1*$^{+/+}$ mice (Figure 7B). Analysis of protein expression from liver lysates also revealed a reduction in IL-6 and Il-1β in HFD-fed *Tbk1*$^{\Delta/\Delta}$ animals compared to *Tbk1*$^{+/+}$ (Figure 7C). Furthermore, WAT and liver protein lysates were analyzed for differences in cytokine expression by multiplex immunoassays. Cytokine levels showed little variance between ND-fed groups, which is consistent with the relatively mild immune phenotype of *Tbk1*$^{\Delta/\Delta}$ animals (Supplemental Fig. 4A,B) [17]. Among the HFD-fed animals, *Tbk1*$^{\Delta/\Delta}$ mice had less cytokine accumulation compared to *Tbk1*$^{+/+}$ mice and in particular, IL-6, IL-1β and TNFα levels were consistently lower in WAT and liver tissues from *Tbk1*$^{\Delta/\Delta}$ mice (Figure 7D,E).

4. DISCUSSION

Numerous studies have demonstrated TBK1 as a key mediator in inflammatory and innate immune responses. However, recent evidence implicating TBK1 in the regulation of insulin receptor activity has emerged, leading us to investigate a novel metabolic function of this serine threonine kinase [21,31–34]. Our data corroborate previously reported upregulation of TBK1 expression on HFD and also show increased pIRF3, indicating heightened TBK1 kinase activity as well. In our DIO model, we confirmed the inhibitory interaction between TBK1 and IRβ and demonstrate that insulin sensitivity is maintained under HFD conditions in the absence of functional TBK1, supporting a previously unappreciated function of TBK1 in regulating insulin receptor activity. *Tbk1*$^{\Delta/\Delta}$ mice are resistant to DIO, and we suspect that this stems primarily from their enhanced insulin sensitivity, allowing for more efficient glucose uptake and utilization. Accordingly, these mice

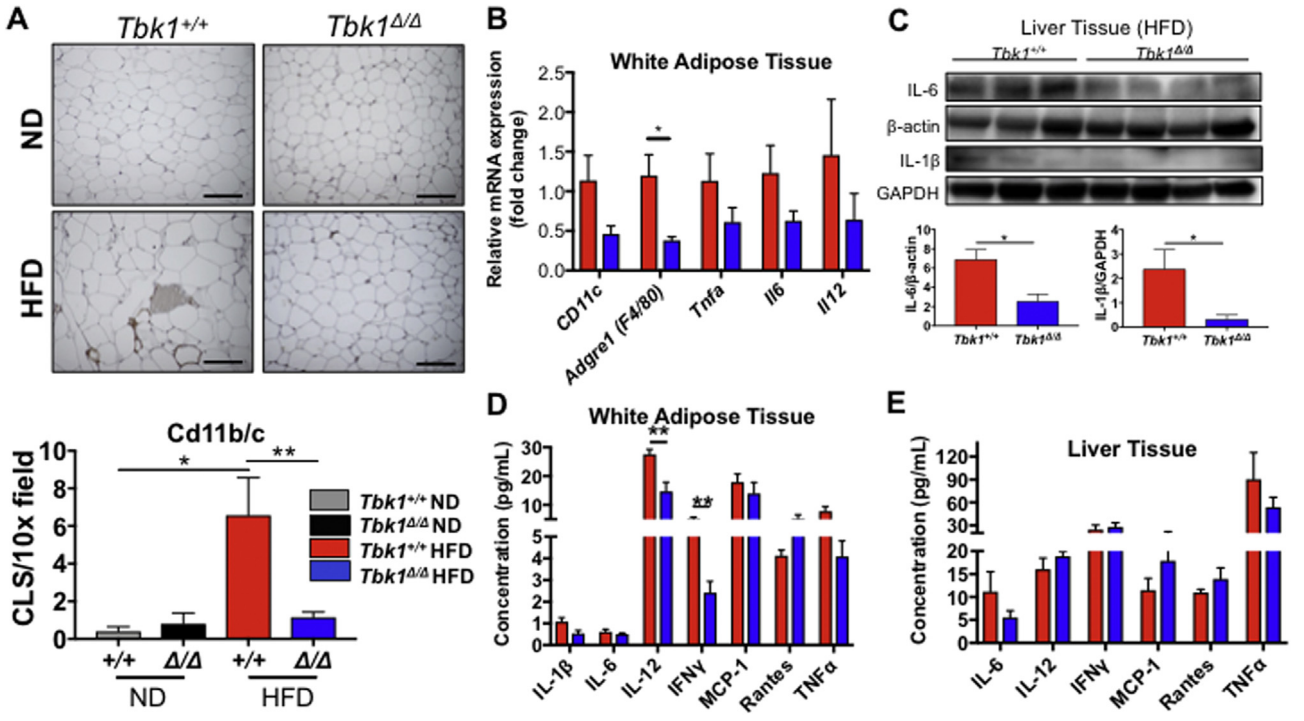

Figure 7: *Tbk1*$^{\Delta/\Delta}$ mice have less inflammation relative to *Tbk1*$^{+/+}$ mice on HFD. **(A)** Representative 20x images and quantification of cd11b/c stained subcutaneous white adipose tissue from *Tbk1*$^{\Delta/\Delta}$ and *Tbk1*$^{+/+}$ mice after 10 weeks on ND or HFD (n = 4–8 mice/group). Scale bar indicates 200 μM and 'CLS' refers to crown like structures. **(B)** mRNA expression of genes encoding CD11c, F4/80, TNFα, IL-6 and IL-12 in subcutaneous WAT of *Tbk1*$^{\Delta/\Delta}$ and *Tbk1*$^{+/+}$ mice fed with HFD as indicated (n = 4–6 mice/group). **(C)** Liver tissue lysates from 14-week-old HFD-fed *Tbk1*$^{\Delta/\Delta}$ and *Tbk1*$^{+/+}$ mice were immunoblotted with antibodies against IL-6 and IL-1β. β-actin and GAPDH were used as internal loading controls. Indicated cytokines from WAT **(D)** and liver tissue **(E)** lysates of HFD-fed *Tbk1*$^{+/+}$ and *Tbk1*$^{\Delta/\Delta}$ mice were measured by Bio-Rad multiplex array (n = 4–8 mice/group for WAT, n = 8–12 mice/group for liver). All mice are from 129S5 background. Results are representative of mean +/− SEM. Statistical analysis by Student's *t*-test. $^{*}p < 0.05$, $^{**}p < 0.01$.

exhibited greater energy expenditure primarily in the form of enhanced physical activity, which accounts for their leaner body composition. These results provide a mechanistic basis for the overall protective effect on the metabolism and general health of *Tbk1*$^{\Delta/\Delta}$ mice challenged with a HFD.

An important consideration with this study is that the *Tbk1*$^{\Delta/\Delta}$ mice contain a global mutation in *Tbk1*, thereby inhibiting its kinase activity and significantly reducing its overall expression in all cell types. Thus, it is unclear if the *Tbk1*$^{\Delta/\Delta}$ mouse phenotype is due to *Tbk1* loss in a specific subset or subsets of tissues or cell types. Interestingly, conditional deletion of *Tbk1* in adipose tissue (*Tbk1 ATKO*) resulted in higher macrophage and proinflammatory cytokine gene expression on HFD [18]. In contrast to our model, HFD-fed *Tbk1 ATKO* mice were insulin resistant and glucose intolerant. This information, in conjunction with the restricted inflammatory response produced by lipopolysaccharide (LPS) stimulated macrophages from the *Tbk1*$^{\Delta/\Delta}$ mice, leads us to speculate whether myeloid cell loss of TBK1 is critical to maintaining insulin sensitivity under metabolic stress [17,35]. In a similar vein, myeloid cell specific knockout of *Ikbkb* (IKKβ gene) in HFD fed mice resulted in improved insulin resistance and lower adiposity, supporting the central contribution of myeloid cells in the development of systemic insulin resistance [7]. With our *Tbk1*$^{\Delta/\Delta}$ model, we conclude that the observed phenotype is the effect of systemically eliminating TBK1 catalytic activity. From a clinical perspective, global loss of TBK1 kinase function could be biologically analogous in some respects to the effects of small molecule inhibition of TBK1 system wide.

The relationship between inflammation and insulin resistance is complex and somewhat controversial. In particular, modulating the expression of certain inflammatory signaling molecules such as IKKβ, JNK, TNFα, IL-1R or IL-6 in different tissues or by different methods has led to inconsistent metabolic outcomes [36]. For example, liver specific JNK activation improved insulin sensitivity, yet activation of JNK in other tissues, including adipose tissue, skeletal muscle and brain, impaired insulin action, suggesting JNK regulation of insulin sensitivity is tissue specific [36–38]. Considering the well-established functions of TBK1 in mediating inflammation and innate immunity, we cannot rule out the possibility that some of the healthier metabolic parameters seen in *Tbk1*$^{\Delta/\Delta}$ mice could be due in part to reduced inflammation, especially given that *Tbk1*$^{\Delta/\Delta}$ macrophages show only a partial response to LPS challenge [17]. While these results are consistent with the argument that inflammation leads to insulin resistance, the scope of this study limits the use of the inflammatory phenotype to function as an indicator of metabolic health in *Tbk1*$^{\Delta/\Delta}$ mice. Regardless, our results strongly suggest that TBK1 promotes metabolic dysfunction through negative regulation of insulin receptor signaling, thus aiding in insulin resistance.

This feature of TBK1 is reminiscent of other kinases that have been previously shown to inhibit insulin signaling in response to cytokine activation. In particular, IKKβ, JNK, PKC, and S6K have each been shown to phosphorylate IRS proteins at unique sites that limit insulin-stimulated activity [26–28]. Accordingly, *S6K1-deficient* mice demonstrate a comparable phenotype to *Tbk1*$^{\Delta/\Delta}$ mice on HFD with lower body weights and insulin hypersensitivity [39,40]. The opposition

of insulin-stimulated anabolic processes common to all of these kinases is indicative of an evolutionary conserved role in reserving energy during times of inflammatory stress for resolving inflammation.

In summary, we have characterized the phenotype of mice globally lacking catalytically active TBK1 under metabolic challenge, which, prior to this mouse, was impossible due to embryonic lethality in *Tbk1*$^{-/-}$ mice [16,17]. Overall, loss of TBK1 kinase activity benefited mice challenged with HFD. One way that TBK1 promotes metabolic syndrome progression is by directly impeding insulin receptor signaling, resulting in systemic insulin resistance and limited glucose absorption. While work from others has begun to elucidate the tissue specific effects of TBK1, it is unclear whether additional TBK1 substrates could be mediating these metabolic effects [18]. A recent study from Kumari and colleagues [41] revealed that the TBK1 substrate IRF3 transcriptionally drives adipose inflammation during periods of overnutrition. IRF3 was upregulated and more active in metabolic tissues from obese mice, matching our observations, while *Irf3*$^{-/-}$ mice were protected from DIO, exhibited reduced inflammation and showed improved insulin sensitivity on HFD. This finding helps elaborate the function of TBK1 under metabolic stress, but also highlights the need for further investigation of TBK1 targets in regulating metabolism.

Lastly, our results, in conjunction with other previous reports, imply that TBK1 inhibition may provide benefits to patients with metabolic syndrome and warrants further testing of pharmacological inhibitors of TBK1 in human trials [14,15,18,42,43]. The TBK1/IKKε inhibitor amlexanox just completed testing in clinical trials beginning with a safety trial of six patients in which no serious adverse events were reported from drug treatment (NCT01842282) [44]. The safety trial was followed by a randomized, double-blind, placebo-controlled trial of 42 obese patients with type 2 diabetes or nonalcoholic fatty liver disease who received amlexanox or placebo for 12 weeks (NCT01975935). A subset of patients constituting one-third of the participants in the blinded study responded with a clinically significant reduction in blood glucose. Interestingly, molecular analysis of fat tissue biopsies collected from patients at the beginning of the study revealed greater inflammation in the responder group compared to non-responders. Though it is unclear whether this high level of inflammation in the responder group showed any sort of resolution by the end of the study, further development and confirmation of this inflammatory gene signature could lead to its utilization as a predictive tool for patient response to amlexanox or potentially other TBK1 inhibitors. Future studies are needed with larger patient groups to validate the efficacy of amlexanox, determine the appropriate dosage and dosing schedule and evaluate whether amlexanox treatment has long-term benefits.

AUTHOR CONTRIBUTIONS

VHC, PES and RAB conceived and designed the study. VHC, ENA and KWW acquired data and performed analysis and interpretation of data. VHC wrote the manuscript. PES and RAB reviewed and revised the manuscript. RAB supervised the study.

ACKNOWLEDGEMENTS

We thank Drs. Risheng Ye and Christine Kusminski for technical advice and shared resources. We also thank Dr. Michael Dellinger for initiating the study and helpful discussions. We gratefully acknowledge Tara Billman and Melissa Gross for their generous assistance with the mouse studies. We also thank Dave Primm for editorial assistance. The work was supported by NIH grants R01 CA192381 to RAB, T32 CA124334 (PI: J. Shay) to VHC and the Effie Marie Cain Scholarship in Angiogenesis Research and the Gillson Longenbaugh Foundation to RAB. The funders had no role in study design, data collection and analysis, decision to publish, or preparation of the manuscript.

CONFLICT OF INTEREST

None declared.

APPENDIX A. SUPPLEMENTARY DATA

Supplementary data related to this article can be found at https://doi.org/10.1016/j.molmet.2018.06.007.

REFERENCES

[1] Poirier, P., Giles, T.D., Bray, G.A., Hong, Y., Stern, J.S., Pi-Sunyer, F.X., et al., 2006. Obesity and cardiovascular disease: pathophysiology, evaluation, and effect of weight loss: an update of the 1997 American heart association scientific statement on obesity and heart disease from the obesity committee of the council on nutrition, physical activity, and metabolism. Circulation 113(6): 898–918.

[2] Wu, H., Ballantyne, C.M., 2017. Skeletal muscle inflammation and insulin resistance in obesity. Journal of Clinical Investigation 127(1):43–54.

[3] Barazzoni, R., Gortan Cappellari, G., Ragni, M., Nisoli, E., 2018. Insulin resistance in obesity: an overview of fundamental alterations. Eating and Weight Disorders 23(2):149–157.

[4] Calay, E.S., Hotamisligil, G.S., 2013. Turning off the inflammatory, but not the metabolic, flames. Nature Medicine 19(3):265–267.

[5] Odegaard, J.I., Chawla, A., 2013. Pleiotropic actions of insulin resistance and inflammation in metabolic homeostasis. Science 339(6116):172–177.

[6] Johnson, A.R., Milner, J.J., Makowski, L., 2012. The inflammation highway: metabolism accelerates inflammatory traffic in obesity. Immunological Reviews 249(1):218–238.

[7] Arkan, M.C., Hevener, A.L., Greten, F.R., Maeda, S., Li, Z.W., Long, J.M., et al., 2005. IKK-beta links inflammation to obesity-induced insulin resistance. Nature Medicine 11(2):191–198.

[8] Uysal, K.T., Wiesbrock, S.M., Marino, M.W., Hotamisligil, G.S., 1997. Protection from obesity-induced insulin resistance in mice lacking TNF-alpha function. Nature 389(6651):610–614.

[9] Weisberg, S.P., Hunter, D., Huber, R., Lemieux, J., Slaymaker, S., Vaddi, K., et al., 2006. CCR2 modulates inflammatory and metabolic effects of high-fat feeding. Journal of Clinical Investigation 116(1):115–124.

[10] Han, M.S., Jung, D.Y., Morel, C., Lakhani, S.A., Kim, J.K., Flavell, R.A., et al., 2013. JNK expression by macrophages promotes obesity-induced insulin resistance and inflammation. Science 339(6116):218–222.

[11] Yuan, M., Konstantopoulos, N., Lee, J., Hansen, L., Li, Z.W., Karin, M., et al., 2001. Reversal of obesity- and diet-induced insulin resistance with salicylates or targeted disruption of Ikkbeta. Science 293(5535):1673–1677.

[12] Hirosumi, J., Tuncman, G., Chang, L., Gorgun, C.Z., Uysal, K.T., Maeda, K., et al., 2002. A central role for JNK in obesity and insulin resistance. Nature 420(6913):333–336.

[13] Baker, R.G., Hayden, M.S., Ghosh, S., 2011. NF-kappaB, inflammation, and metabolic disease. Cell Metabolism 13(1):11–22.

[14] Chiang, S.H., Bazuine, M., Lumeng, C.N., Geletka, L.M., Mowers, J., White, N.M., et al., 2009. The protein kinase IKKepsilon regulates energy balance in obese mice. Cell 138(5):961–975.

[15] Reilly, S.M., Chiang, S.H., Decker, S.J., Chang, L., Uhm, M., Larsen, M.J., et al., 2013. An inhibitor of the protein kinases TBK1 and IKK-varepsilon improves obesity-related metabolic dysfunctions in mice. Nature Medicine 19(3):313–321.

[16] Bonnard, M., Mirtsos, C., Suzuki, S., Graham, K., Huang, J., Ng, M., et al., 2000. Deficiency of T2K leads to apoptotic liver degeneration and impaired NF-kappaB-dependent gene transcription. The EMBO Journal 19(18):4976–4985.

[17] Marchlik, E., Thakker, P., Carlson, T., Jiang, Z., Ryan, M., Marusic, S., et al., 2010. Mice lacking Tbk1 activity exhibit immune cell infiltrates in multiple tissues and increased susceptibility to LPS-induced lethality. Journal of Leukocyte Biology 88(6):1171–1180.

[18] Zhao, P., Wong, K.I., Sun, X., Reilly, S.M., Uhm, M., Liao, Z., et al., 2018. TBK1 at the crossroads of inflammation and energy homeostasis in adipose tissue. Cell 172(4):731–743 e712.

[19] Rotter, V., Nagaev, I., Smith, U., 2003. Interleukin-6 (IL-6) induces insulin resistance in 3T3-L1 adipocytes and is, like IL-8 and tumor necrosis factor-alpha, overexpressed in human fat cells from insulin-resistant subjects. Journal of Biological Chemistry 278(46):45777–45784.

[20] Eder, K., Baffy, N., Falus, A., Fulop, A.K., 2009. The major inflammatory mediator interleukin-6 and obesity. Inflammation Research 58(11):727–736.

[21] Munoz, M.C., Giani, J.F., Mayer, M.A., Toblli, J.E., Turyn, D., Dominici, F.P., 2009. TANK-binding kinase 1 mediates phosphorylation of insulin receptor at serine residue 994: a potential link between inflammation and insulin resistance. Journal of Endocrinology 201(2):185–197.

[22] Strack, V., Stoyanov, B., Bossenmaier, B., Mosthaf, L., Kellerer, M., Haring, H.U., 1997. Impact of mutations at different serine residues on the tyrosine kinase activity of the insulin receptor. Biochemical and Biophysical Research Communications 239(1):235–239.

[23] Strack, V., Hennige, A.M., Krutzfeldt, J., Bossenmaier, B., Klein, H.H., Kellerer, M., et al., 2000. Serine residues 994 and 1023/25 are important for insulin receptor kinase inhibition by protein kinase C isoforms beta2 and theta. Diabetologia 43(4):443–449.

[24] Maher, J.J., Leon, P., Ryan, J.C., 2008. Beyond insulin resistance: innate immunity in nonalcoholic steatohepatitis. Hepatology 48(2):670–678.

[25] McLaughlin, T., Ackerman, S.E., Shen, L., Engleman, E., 2017. Role of innate and adaptive immunity in obesity-associated metabolic disease. Journal of Clinical Investigation 127(1):5–13.

[26] Saltiel, A.R., Olefsky, J.M., 2017. Inflammatory mechanisms linking obesity and metabolic disease. Journal of Clinical Investigation 127(1):1–4.

[27] Copps, K.D., White, M.F., 2012. Regulation of insulin sensitivity by serine/threonine phosphorylation of insulin receptor substrate proteins IRS1 and IRS2. Diabetologia 55(10):2565–2582.

[28] Haeusler, R.A., McGraw, T.E., Accili, D., 2018. Biochemical and cellular properties of insulin receptor signalling. Nature Reviews Molecular Cell Biology 19(1):31–44.

[29] Hay, N., 2011. Akt isoforms and glucose homeostasis - the leptin connection. Trends in Endocrinology and Metabolism 22(2):66–73.

[30] Sun, K., Kusminski, C.M., Scherer, P.E., 2011. Adipose tissue remodeling and obesity. Journal of Clinical Investigation 121(6):2094–2101.

[31] Helgason, E., Phung, Q.T., Dueber, E.C., 2013. Recent insights into the complexity of Tank-binding kinase 1 signaling networks: the emerging role of cellular localization in the activation and substrate specificity of TBK1. FEBS Letters 587(8):1230–1237.

[32] Chen, H., Sun, H., You, F., Sun, W., Zhou, X., Chen, L., et al., 2011. Activation of STAT6 by STING is critical for antiviral innate immunity. Cell 147(2):436–446.

[33] Hacker, H., Karin, M., 2006. Regulation and function of IKK and IKK-related kinases. Science STKE 2006(357):re13.

[34] Fitzgerald, K.A., McWhirter, S.M., Faia, K.L., Rowe, D.C., Latz, E., Golenbock, D.T., et al., 2003. IKKepsilon and TBK1 are essential components of the IRF3 signaling pathway. Nature Immunology 4(5):491–496.

[35] Yu, T., Yi, Y.S., Yang, Y., Oh, J., Jeong, D., Cho, J.Y., 2012. The pivotal role of TBK1 in inflammatory responses mediated by macrophages. Mediators of Inflammation 2012:979105.

[36] Ye, J., McGuinness, O.P., 2013. Inflammation during obesity is not all bad: evidence from animal and human studies. American Journal of Physiology. Endocrinology and Metabolism 304(5):E466–E477.

[37] Sabio, G., Kennedy, N.J., Cavanagh-Kyros, J., Jung, D.Y., Ko, H.J., Ong, H., et al., 2010. Role of muscle c-Jun NH2-terminal kinase 1 in obesity-induced insulin resistance. Molecular and Cellular Biology 30(1):106–115.

[38] Jurczak, M.J., Lee, A.H., Jornayvaz, F.R., Lee, H.Y., Birkenfeld, A.L., Guigni, B.A., et al., 2012. Dissociation of inositol-requiring enzyme (IRE1-alpha)-mediated c-Jun N-terminal kinase activation from hepatic insulin resistance in conditional X-box-binding protein-1 (XBP1) knock-out mice. Journal of Biological Chemistry 287(4):2558–2567.

[39] Um, S.H., Frigerio, F., Watanabe, M., Picard, F., Joaquin, M., Sticker, M., et al., 2004. Absence of S6K1 protects against age- and diet-induced obesity while enhancing insulin sensitivity. Nature 431(7005):200–205.

[40] Um, S.H., Sticker-Jantscheff, M., Chau, G.C., Vintersten, K., Mueller, M., Gangloff, Y.G., et al., 2015. S6K1 controls pancreatic beta cell size independently of intrauterine growth restriction. Journal of Clinical Investigation 125(7):2736–2747.

[41] Kumari, M., Wang, X., Lantier, L., Lyubetskaya, A., Eguchi, J., Kang, S., et al., 2016. IRF3 promotes adipose inflammation and insulin resistance and represses browning. Journal of Clinical Investigation 126(8):2839–2854.

[42] Mowers, J., Uhm, M., Reilly, S.M., Simon, J., Leto, D., Chiang, S.H., et al., 2013. Inflammation produces catecholamine resistance in obesity via activation of PDE3B by the protein kinases IKKepsilon and TBK1. Elife 2:e01119.

[43] Reilly, S.M., Ahmadian, M., Zamarron, B.F., Chang, L., Uhm, M., Poirier, B., et al., 2015. A subcutaneous adipose tissue-liver signalling axis controls hepatic gluconeogenesis. Nature Communications 6:6047.

[44] Oral, E.A., Reilly, S.M., Gomez, A.V., Meral, R., Butz, L., Ajluni, N., et al., 2017. Inhibition of IKKvarepsilon and TBK1 improves glucose control in a subset of patients with type 2 diabetes. Cell Metabolism 26(1):157–170 e157.

